AIP Advances

Full correspondence between asymmetric filling of slits and first-order phase transition lines

Leszek Szybisz and Salvador A. Sartarelli

Citation: AIP Advances **1**, 042146 (2011); doi: 10.1063/1.3664297
View online: http://dx.doi.org/10.1063/1.3664297
View Table of Contents: http://aipadvances.aip.org/resource/1/AAIDBI/v1/i4
Published by the American Institute of Physics.

Full correspondence between asymmetric filling of slits and first-order phase transition lines

Leszek Szybisz[1,2,3,a] and Salvador A. Sartarelli[4]
[1]*Laboratorio TANDAR, Departamento de Física, Comisión Nacional de Energía Atómica, Av. del Libertador 8250, RA–1429 Buenos Aires, Argentina*
[2]*Departamento de Física, Facultad de Ciencias Exactas y Naturales, Universidad de Buenos Aires, Ciudad Universitaria, RA–1428 Buenos Aires, Argentina*
[3]*Consejo Nacional de Investigaciones Científicas y Técnicas, Av. Rivadavia 1917, RA–1033 Buenos Aires, Argentina*
[4]*Instituto de Desarrollo Humano, Universidad Nacional de General Sarmiento, Gutierrez 1150, RA–1663 San Miguel, Argentina*

(Received 13 September 2011; accepted 24 October 2011; published online 14 November 2011)

Adsorption on single planar walls and filling of slits with identical planar walls are investigated in the frame of the density functional theory. In this sort of slits the external potential is symmetric with respect to its central plane. Calculations were carried out by applying both the canonical and grand canonical ensembles (CE and GCE, respectively). The behavior is analyzed by varying the strength of the adsorbate-substrate attraction, the temperature T, and the coverage Γ_ℓ. Results obtained for physisorption of Xe on alkaline surfaces are reported in the present work. Prewetting (PW) lines and wetting temperatures, T_w, are determined from the analysis of adsorption on single walls. The filling of slits is analyzed for temperatures $T > T_w$. It is found that whenever for a given Xe-substrate combination the adsorption on a single wall exhibits a first-order wetting transition then asymmetric profiles that break the left-right symmetry of the external potential appear in the filling of an equivalent slit. These spontaneously symmetry breaking (SSB) solutions occur in a restricted range of Γ_ℓ with a T-dependent width. In the case of closed slits analyzed in the CE scheme, the obtained asymmetric profiles exhibit lower Helmholtz free energies than the symmetric species and, therefore, could be stabilized in this geometry. For open slits, the GCE scheme yields all the symmetric and SSB states in the corresponding convex regimes of the free energy. It is shown that both the CE and the GCE frames yield three coexistent states, two symmetric and one asymmetric twofold degenerate. Both a PW line and the related SSB effect terminate at the same temperature. For rather strongly attractive surfaces reentrant SSB states are found at a fixed value of T. [doi:10.1063/1.3664297]

I. INTRODUCTION

The study of the adsorption of fluids on solid walls is of considerable current interest. An entire volume including reviews and discussions of theoretical and experimental investigations on this subject was recently published.[1] That set of articles indicates that properties of systems involving fluids at interfaces, like wetting, spreading and filling, are not only interesting from the fundamental physics point of view, but have also numerous technological applications. Namely, these systems consist of a liquid phase (l) adsorbed on solid substrates (s) in the presence of a vapor atmosphere

[a]Electronic mail: szybisz@tandar.cnea.gov.ar

(v). Its behavior depends on: the strength of the fluid-fluid (*f-f*) attraction, ε_{ff}, the well depth of the substrate-fluid (*s-f*) interaction, $\mathcal{W}_{sf}$, the temperature, T, and the chemical potential, μ.

A systematic classification of the adsorption on attractive planar surfaces, which exhibit an infinite extent in the x and y directions, was performed by Pandit, Schick, and Wortis.[2] In practice, at a fixed T the adsorption properties are mainly determined by the relative strength $\varepsilon_r = \mathcal{W}_{sf}/\varepsilon_{ff}$. By varying this parameter it is possible to sweep a variety of physical phenomena like drying, critical wetting, prewetting, wetting, and layer formation. Given a value of ε_r, the results are usually summarized as a phase diagram in the (T, μ) plane, typical examples are depicted in Fig. 1 of Ref. 3. For moderate substrates (i.e., when ε_r is slightly bigger than one) there is a first-order wetting transition at the point [T_w, $\mu_w = \mu_0(T_w)$] between the triple point temperature, T_t, and the critical one, T_c. In this case T_w is characterized by the appearance of coexisting thin and very thick adsorbed fluid films, while for $T < T_w$ the coverage of adsorbed films is finite (incomplete wetting). Under these conditions for $T \geq T_w$ there is an associated prewetting (PW) line which extends away from [T_w, μ_w] into the region of pressures below the corresponding bulk saturation value $P_0(T)$ and terminates at the critical prewetting (CPW) point [T_{cpw}, μ_{cpw}], see Fig. 1(b) in Ref. 3. It is usually assumed that in this regime the density profile of the fluid only depends on the coordinate z perpendicular to the substrate, $\rho(\mathbf{r}) = \rho(z)$. A PW transition is marked by a jump in the excess surface density (coverage), often expressed in nominal layers ℓ as

$$\Gamma_\ell = (1/\rho_l^{2/3}) \int_0^\infty dz[\rho(z) - \rho_B] \,, \tag{1}$$

where ρ_B is the asymptotic bulk vapor density and ρ_l the liquid density at saturation for a given temperature. The discontinuity in Γ_ℓ vanishes at T_{cpw}, where the coexisting thin and thick films become identical. For slightly more attractive substrates the phase diagram presents several convergent PW lines like in Fig. 1(d) of Ref. 3. In the case of strong substrates the coverage increases from zero, either in monolayer steps or continuously.

If a fluid is adsorbed on a single planar wall the physisorption potential does not exhibit any symmetry along the z axis perpendicular to the substrate. On the other hand, when the confinement is produced by a planar slit with identical walls the *s-f* interaction becomes symmetric with respect to the plane located at the center of the slit. Under such conditions it is quite reasonable to expect that $\rho(z)$ would respect the symmetry of the external potential. However, Sikkenk *et al.*[4,5] have found by carrying out molecular dynamics calculations that asymmetric density profiles of the fluid may appear in the process of filling a planar slit built up of moderately attractive identical walls. This phenomenon is known as spontaneous symmetry breaking (SSB) effect and disappears above a critical temperature T_{sb}. The authors of Ref. 4 explained the occurrence of structures with different symmetries in terms of the balance of substrate-liquid γ_{sl}, substrate-vapor γ_{sv}, and liquid-vapor γ_{lv} surface tensions. The SSB effect has been analyzed over more than two decades. In most of the studies, a Canonical Ensemble (CE) statistics was applied to examine filling of closed slits with classical gases.[6–12] Recently, Berim and Ruckenstein[13] have also investigated the occurrence of SSB for quantum ^{4}He confined in planar slits.

Furthermore, this kind of asymmetric solutions were also found by Merkel and Löwen in open systems.[14] By using both computer simulations and density functional (DF) theory in the frame of the Grand Canonical Ensemble (GCE) these authors demonstrated that under certain conditions a system confined by a symmetric potential can reach a state where the fluid shows a liquid-like density on one side and vapor-like density on the other side. Further evidence for symmetry breaking may be found in the works reported by Rżysko *et al.*[15] who carried out Monte Carlo simulations and by Edison and Monson who applied a dynamic mean field theory.[16]

Wetting and filling are intimately related phenomena. In a recent simultaneous study of wetting and filling we found some evidence for a correspondence between T_{cpw} of a single PW line obtained in the case of one wall adsorption and T_{sb} determined for the disappearance of SSB in slits.[10,12] Moreover, Rżysko *et al.*[15] have also suggested that the SSB is a result of the first-order nature of the transition. If the transition were of the second order, SSB would not occur. It is the aim of the present work to report a systematic search for establishing a general relation between PW and SSB. The behavior as a function of ε_r and T was examined. It was found that: whenever for a given

adsorbate-substrate combination the adsorption on a single planar wall exhibits a first-order wetting transition then asymmetric profiles appear by filling an equivalent slit, and both these phenomena PW and SSB terminate at the same temperature.

The theoretical background is outlined in Sec. II. Section III is devoted to present and analyze the results of our calculations performed in the frames of both the CE and GCE statistics. A summary of the findings is provided in Sec. IV.

II. THEORETICAL FRAME

To establish a reliable correspondence between wetting and filling both kind of systems are treated in exactly the same approach. The present calculations have been carried out in the frame of the DF theory recently applied for studying physical adsorption of Ne and Ar.[10–12,17,18] This theory is based on the existence of a grand canonical functional $\Omega(T, \mu, [\rho(\mathbf{r})])$ of the one-particle density $\rho(\mathbf{r})$ in the (one-component) system, which depends parametrically on the two thermodynamic variables T and μ[19]

$$\Omega(T, \mu, [\rho(\mathbf{r})]) = F_{\rm DF}(T, [\rho(\mathbf{r})]) - \mu N \ , \tag{2}$$

where $F_{\rm DF}$ is the functional for the Helmholtz free energy and N the number of adatoms

$$N = \int \rho(\mathbf{r})\, \mathbf{dr} \ . \tag{3}$$

The equilibrium density profile $\rho_e(\mathbf{r})$ of the adsorbed fluid is obtained by solving the Euler-Lagrange (E-L) equation derived by minimizing (at fixed T and μ) the grand thermodynamic potential

$$\left. \frac{\delta \Omega(T, \mu, [\rho])}{\delta \rho(\mathbf{r})} \right|_{\rho = \rho_e(\mathbf{r})} = 0 \ . \tag{4}$$

The value of the functional at equilibrium, $\Omega(T, \mu, [\rho = \rho_e])$ is the real equilibrium grand canonical free energy Ω_e.

A. Density functional

In the DF theory there is no recipe for an exact expression of the intrinsic free energy $F_{\rm DF}$ corresponding to a fluid immersed in an external potential $U_{sf}(\mathbf{r})$.[20] We adopted the following form

$$\begin{aligned} F_{\rm DF}(T, [\rho(\mathbf{r})]) = \nu_{\rm id}\, k_B\, T \int d\mathbf{r}\, \rho(\mathbf{r}) \{\ln[\Lambda^3 \rho(\mathbf{r})] - 1\} \\ + \int d\mathbf{r}\, \rho(\mathbf{r})\, \Delta f_{\rm HS}[\bar{\rho}(\mathbf{r}); d_{\rm HS}] \\ + \frac{1}{2} \int \int d\mathbf{r}\, d\mathbf{r}' \rho(\mathbf{r})\, \rho(\mathbf{r}') \Phi_{\rm attr}(|\, \mathbf{r} - \mathbf{r}'\, |) \\ + \int d\mathbf{r}\, \rho(\mathbf{r})\, U_{sf}(\mathbf{r}) \ . \end{aligned} \tag{5}$$

The first term is the ideal gas free energy, where k_B is the Boltzmann constant and Λ the de Broglie thermal wavelength. Factor $\nu_{\rm id}$ was introduced by Ancilotto and collaborators in Eq. 4 of Ref. 21 (in a standard theory it is equal to unity). The second term is the repulsive *f-f* interaction approximated by a hard-sphere (HS) fundamental measure theory (FMT) functional taken from Kierlik and Rosinberg[22] (KR), which has proven to be very successful even in highly inhomogeneous situations. Here $d_{\rm HS}$ is the HS diameter. The KR version is completely equivalent to the original FMT devised by Rosenfeld.[23] Notice that in the literature there are more recent versions of the FMT formulation like, for instance, the White Bear proposal[24] where the Mansoori-Carnahan-Starling-Leland[25] bulk equation of state was included. This fact makes the White Bear version more adequate for studying binary mixtures, but in the case of one-component HS fluid the difference with the original Rosenfeld functional is negligible as depicted in Fig. 3 of Ref. 24. The third term is the

attractive *f-f* interaction treated in a mean-field approximation (MFA), which is written in terms of a recently proposed version[17] of the separation of the spherically symmetric Lennard-Jones (LJ) 12-6 potential originally introduced by Weeks, Chandler, and Andersen[26] (WCA)

$$\Phi_{\rm attr}^{\rm WCA}(r) = \begin{cases} -\tilde{\varepsilon}_{ff} \ , & r \le r_m \\ 4\tilde{\varepsilon}_{ff}\left[\left(\frac{\tilde{\sigma}_{ff}}{r}\right)^{12} - \left(\frac{\tilde{\sigma}_{ff}}{r}\right)^{6}\right] , & r > r_m \ , \end{cases} \tag{6}$$

where $r = |\mathbf{r} - \mathbf{r}'|$ and $r_m = 2^{1/6}\tilde{\sigma}_{ff}$ is the position of the LJ minimum. We set $d_{\rm HS} = \tilde{\sigma}_{ff}$. The last contribution to Eq. (5) is due to the adsorbate-substrate interaction.

The well depth $\tilde{\varepsilon}_{ff}$ and interaction size $\tilde{\sigma}_{ff}$ are considered as free parameters because the use of its standard bare values $\varepsilon_{\rm XeXe}/k_B = 221$ K and $\sigma_{\rm XeXe} = 4.1$ Å (see, e.g., Ref. 27) overestimates the experimental result $T_c = 289.74$ K. The three adjustable parameters (namely, ν_{rn}, $\tilde{\varepsilon}_{ff}$, and $\tilde{\sigma}_{ff}$) were simultaneously determined by imposing that on the *l-v* coexistence curve of Xe at a fixed T the data of $\rho_l(T)$, $\rho_v(T)$, and $P_0(T) = P(\rho_l) = P(\rho_v)$ listed in Table XXIII of Ref. 28 be reproduced. In addition, since two bulk phases can coexist at a given T if and only if their chemical potentials are equal at P_0, i.e.,

$$\mu_l(T, P_0) = \mu_v(T, P_0) = \mu_0(T) \ , \tag{7}$$

therefore, we also imposed this condition. For determining the optimal $\tilde{\sigma}_{ff}$ all the contributions to the Helmholtz free energy containing this parameter, i.e., all the corresponding terms in both the $\Delta f_{\rm HS}[\bar{\rho}(\mathbf{r}); d_{\rm HS} = \tilde{\sigma}_{ff}]$ and $\Phi_{\rm attr}^{\rm WCA}(r; \tilde{\varepsilon}_{ff}, \tilde{\sigma}_{ff})$ energies were considered. The obtained parameter $\nu_{\rm id}$ is essentially unity near T_t and decreases to about 0.9 in the regime close to T_c where there is a well known departure from the ideal gas behavior.[29] Since $\nu_{\rm id}$ is not strictly unity the Henry's law for adsorption at very low densities[30] is slightly violated in the present formulation. All in all, the present DF version should be considered as a relatively easy phenomenological approach with parameters introduced to account for experimental bulk data.

B. Euler-Lagrange equations

The equilibrium density profile $\rho(\mathbf{r})$ of the fluid is determined from the variational Eq. (4) written as

$$\frac{\delta}{\delta\rho(\mathbf{r})}\left[F_{\rm DF}[\rho(\mathbf{r}')] - \mu \int d\mathbf{r}' \, \rho(\mathbf{r}')\right] = 0 \ . \tag{8}$$

This functional minimization leads to

$$\frac{\delta[F_{\rm DF}(T, [\rho(\mathbf{r}')])]}{\delta\rho(\mathbf{r})} = \mu \ . \tag{9}$$

This variational condition yields the following E-L equation for a planar geometry

$$\nu_{\rm id}\, k_B\, T \ \ln\left[\Lambda^3\, \rho(z)\right] + Q(z) = \mu \ , \tag{10}$$

with

$$\begin{aligned} Q(z) = {} & \Delta f_{\rm HS}[\bar{\rho}(z); d_{\rm HS}] \\ & + \int_0^L dz' \, \rho(z') \, \frac{\delta \Delta f_{\rm HS}[\bar{\rho}(z'); d_{\rm HS}]}{\delta \bar{\rho}(z')} \, \frac{\delta \bar{\rho}(z')}{\delta \rho(z)} \\ & + \int_0^L dz' \, \rho(z') \, \bar{\Phi}_{\rm attr}(|\, z - z' \,|) + U_{sf}(z) \ . \end{aligned} \tag{11}$$

Here L is the size of the box adopted for solving the E-L equation. In addition, the number of particles by wall's area A becomes

$$n = N/A = \int_0^L \rho(z) dz. \tag{12}$$

1. Grand canonical ensemble

In an experimental setup devised to investigate adsorption, the fluid is usually exposed to a reservoir at fixed T_{bath} and P_{bath} (i.e., μ_{bath}) allowing an unrestricted particle exchange with the environment. Under such conditions, the system at thermodynamic equilibrium exhibits fixed V, $T = T_{bath}$, and $\mu = \mu_{bath}$, hence, the adequate procedure for studying such a phenomenon is to apply the GCE statistics. In such a scheme the E-L equation should be solved by fixing μ and searching for the optimal solutions for $\rho(z)$ and $n = N/A$.

Given a value of the independent variable μ the density profile may be evaluated by inverting Eq. (10)

$$\rho(z) = \frac{1}{\Lambda^3} \exp\left(\frac{\mu - Q(z)}{\nu_{\rm id}\, k_B\, T}\right), \tag{13}$$

and the self-consistent solution is obtained iterating this relation up to convergence. The number of particles per unit area is calculated with the expression

$$n = \frac{1}{\Lambda^3} \exp\left(\frac{\mu}{\nu_{\rm id}\, k_B\, T}\right) \int_0^L dz \, \exp\left(-\frac{Q(z)}{\nu_{\rm id}\, k_B\, T}\right). \tag{14}$$

2. Canonical ensemble

However, in practice, it is usual[7,8,35] to solve the adsorption problem by fixing n together with V and T, that is by applying the CE scheme, which is much easier to manage numerically than the GCE one. Notice that μ and n are conjugate Legendre variables. In the CE statistics (strictly valid for closed systems) μ is treated as a Lagrange multiplier μ_{ce} to be determined from the solutions together with $\rho(z)$. So, in this case one should solve

$$\frac{\delta[F_{\rm DF}(T, [\rho(z')])]}{\delta\rho(z)} = \mu_{ce}\ , \tag{15}$$

which leads to the E-L equation

$$\nu_{\rm id}\, k_B\, T\ \ln\left[\Lambda^3\, \rho(z)\right] + Q(z) = \mu_{ce}\ . \tag{16}$$

Then, the density profile $\rho(z)$ can be written as

$$\rho(z) = \rho_0 \exp\left(-\frac{Q(z)}{\nu_{\rm id}\, k_B\, T}\right), \tag{17}$$

with

$$\rho_0 = \frac{1}{\Lambda^3} \exp\left(\frac{\mu_{ce}}{\nu_{\rm id}\, k_B\, T}\right). \tag{18}$$

Since in the CE scheme the calculations are performed at a fixed n, whilst μ_{ce} is an unknown quantity, then Eq. (18) is used to evaluate μ_{ce} and ρ_0 is obtained from the integrated density profile

$$n = \rho_0 \int_0^L dz \, \exp\left(-\frac{Q(z)}{\nu_{\rm id}\, k_B\, T}\right), \tag{19}$$

which leads to

$$\rho_0 = \frac{n}{\int_0^L dz \, \exp\left(-\frac{Q(z)}{\nu_{\rm id}\, k_B\, T}\right)}\ . \tag{20}$$

Equating expressions (17), (18) and (20) one gets

$$\rho(z) = \frac{n}{\int_0^L dz \, \exp\left(-\frac{Q(z)}{\nu_{\rm id}\, k_B\, T}\right)} \exp\left(-\frac{Q(z)}{\nu_{\rm id}\, k_B\, T}\right) \tag{21}$$

for the density profile and

$$\mu_{ce} = -\nu_{\rm id}\, k_B\, T\, \ln\left[\frac{1}{n\,\Lambda^3}\int_0^L dz\, \exp\left(-\frac{Q(z)}{\nu_{\rm id}\, k_B\, T}\right)\right] \tag{22}$$

for the chemical potential. In this scheme, $\rho(z)$ is determined by iterating Eq. (21) until the required convergence is achieved, then μ_{ce} is calculated with Eq. (22).

III. ANALYSIS OF THE ADSORPTION

Before entering into the analysis of physisorption, we validated the obtained parameters by evaluating the surface tension of the free liquid-vapor interface, γ_{lv}. For such a purpose we set $U_{sf}(z) = 0$ and followed the procedure outlined in previous works. Along the calculations dimensionless variables $z^* = z/\tilde{\sigma}_{ff}$ and $L^* = L/\tilde{\sigma}_{ff}$ for distances, $n^* = N\tilde{\sigma}_{ff}^2/A$ for areal density, and $\rho^* = \rho\,\tilde{\sigma}_{ff}^3$ for volume density are used.[17,18] Our results for γ_{lv} agree very well (in a similar way as for Ne and Ar in the latter references) with experimental data[31] over the entire temperature range $T_t(= 161.3\ \text{K}) \leq T \leq T_c$.

For the analysis of physisorption we adopted in all the cases the *ab initio* potentials of Chismeshya, Cole, and Zaremba (CCZ), $U_{\rm CCZ}(z)$, given by Eq. (3) in Ref. 32 with the potential parameters listed in Table 1 therein. We report here results for adsorption of Xe on surfaces of Na, Li, and Mg. This set of substrates with $\varepsilon_r = \mathcal{W}_{s\rm Xe}/\varepsilon_{\rm XeXe} = 2.1$, 2.8, and 5.5, respectively, displays different wetting scenarios. Let us mention that Sinanoğlu and Pitzer[33] suggested that the strength of the pair *f-f* potential is modified by interactions with solid substrates. This effect is discussed in detail in Ref. 34. In the present paper, we neglect the adsorption-induced interactions and, along with other earlier authors,[13,21,35–37] adopt for studying physisorption the pair *f-f* potential of Eq. (6) with the empirical parameters $\tilde{\varepsilon}_{\rm XeXe}$ and $\tilde{\sigma}_{\rm XeXe}$ determined in the previous section.

In a first step we shall study adsorption on a single wall in order to determine PW lines and T_w temperatures. In so doing methods of analysis will be outlined, which will be also utilized for examining filling of pore slits.

A. Adsorption on a single wall

In this geometry the E-L equation was solved for $U_{sf}(z) = U_{\rm CCZ}(z)$ in a box of size $L^* = 40$. Adsorption isotherms at fixed temperatures, i.e., the reduced chemical potential $\Delta\mu(T) = \mu(T) - \mu_0(T)$ and Γ_ℓ were calculated using both the GCE and CE schemes.

Let us outline the treatment of the obtained results by describing the analysis of the adsorption isotherm for Xe deposited on Na at the highest temperature at which a van der Waals loop is observed. So, data calculated at $T = 245$ K are displayed in Fig. 1. The solid lines stand for results obtained with both the GCE and CE calculations. Between the spinodal points S_1 and S_2 (characterized by $d\mu/dn = 0$) there is a region marked by a dashed curve where $d\mu/dn < 0$. In that regime $F_{\rm DF}$ is not convex and the data were obtained from CE calculations. The GCE scheme only provides solutions with positive slope $d\mu/dn$ guaranteeing convexity of $F_{\rm DF}$. Notice, that this property is also exhibited by variational microscopic calculations performed in the framework of the paired-phonon analysis in conjunction with the hyper-netted chain expansion.[38–41]

In practice, to get convergence in the CE scheme one needs a smaller number of iterations than in the GCE case. This feature is due to the fact that at each step of the CE procedure $\rho(z)$ is normalized to the required number of particles. Therefore, the CE scheme is widely used in the literature to study adsorption. A theoretical justification for the broad use of CE was provided by White *et al.*[42] These authors have shown that for stable or metastable solutions the results of the GCE and CE statistics may differ only if one considers situations of extreme confinement with a small number of particles.

The CE scheme provides $\Delta\mu(T)$ for all values of n. When in this frame the data exhibit van der Waals loops, the two coexistent stable states located at n_{min} and n_{max} (i.e., at $\Gamma_{\ell,\,min}$ and $\Gamma_{\ell,\,max}$,

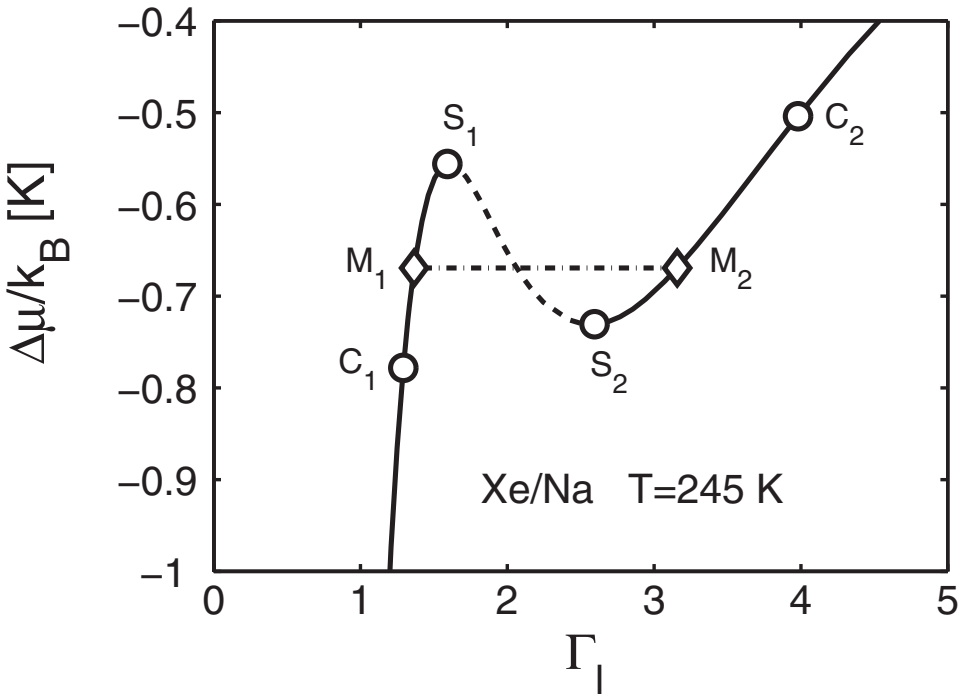

FIG. 1. Adsorption isotherm for Xe adsorbed on a single wall of Na at $T = 245$ K. Solid curves were obtained with both the GCE and CE schemes, while the dashed line is obtained in the CE scheme only. Labels S_1 and S_2 show the location of spinodal points, while C_1 and C_2 are two generic stable states in the thin and thick film regimes, respectively. M_1 and M_2 stand for the coexistent thin and thick films determined from Maxwell construction indicated by the dash-dotted line.

respectively) which satisfy

$$\mu(n_{min}) = \mu(n_{max}) = \mu_e(\Omega_e/A) \tag{23}$$

are determined by applying the Maxwell's rule of equal areas as in Refs. 17, 35 and 43

$$\int_{n_{min}}^{n_{max}} [\mu(T) - \mu_0(T)]dn = \Delta\mu_{pw}(T)[n_{max} - n_{min}] \, . \tag{24}$$

For $n \leq n_{min}$ the system grows continuously. In this case, for $n \geq n_{max}$ (i.e., for $\Gamma_\ell \geq \Gamma_{\ell,\,max}$) the film's growth does not present any further jump in coverage, for stronger substrates multiple jumps may occur (see below results for the Xe/Li system).

In the case of the GCE scheme, it is impossible to apply the equal area Maxwell's rule given by Eq. (24) due to the lack of data in the non convex region. Hence, some other method should be utilized to get the coexistent states. In the following lines we shall outline an adequate procedure.

The thermodynamics of a surface system is specified by the differential form for the free energy[40,41]

$$dF = d(E - TS) = -S\,dT + \gamma\,dA + \mu\,dN \, . \tag{25}$$

Here E is the total internal energy and γ the total surface tension (or surface energy per unit area). At a fixed T and constant A one gets

$$\mu = \left(\frac{\partial F}{\partial N}\right)_{T,A} = f + n\,\frac{\partial f}{\partial n} \, , \tag{26}$$

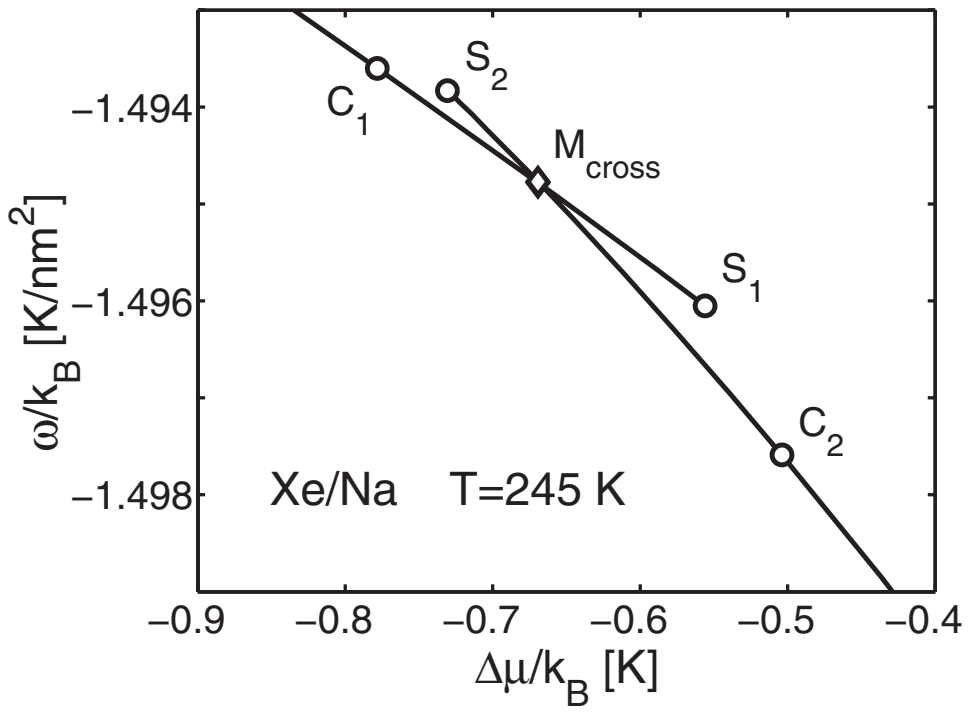

FIG. 2. Grand potential per unit area as function of the chemical potential for Xe adsorbed on a single wall of Na at $T = 245$ K. Data were obtained in the GCE scheme. The curve containing the C_1 and S_1 points correspond to thin films, while that with S_2 and C_2 points to thick films. The crossing point labeled by M_{cross} indicate the coexistent thin and thick films.

and at constant N

$$\gamma = \left(\frac{\partial F}{\partial A}\right)_{T,N} = \frac{\partial f}{\partial n^{-1}} = -n^2 \frac{\partial f}{\partial n} = n\,(f - \mu)$$
$$= \frac{F - \mu N}{A} = \frac{\Omega}{A} = \omega\ . \tag{27}$$

The equilibrium conditions for a single-component fluid at T are that γ and μ be uniform throughout the system. Therefore, two phases can coexist at a given T if and only if as required by Eq. (23) for some μ_e both phases have the same γ_e (in other words equal ω_e). From a set $(n, \mu, f_{\rm DF})$ obtained in the convex regime of $F_{\rm DF}$, i.e. along the sectors C_1-S_1 and S_2-C_2 of the curves traced in Fig. 1, one can evaluate ω, and in turn these data can be used to perform the "so called" tangent Maxwell construction.[44] In practice, knowing μ and ω as a function of n one can plot ω vs. $\Delta\mu$ and determine μ_e and ω_e at coexistence. See, for instance, the crossing diagram plotted in Fig. 3 of Ref. 40 and the zigzag constructions displayed in Fig. 5(b) of Ref. 16 and in Fig. 2 of Ref. 43. Our data are plotted in Fig. 2, where the crossing point labeled by M_{cross} determines $\Delta\mu_{pw}(T)$ and ω_{pw} at coexistence. At this crossing point there is a knee characteristic of a first-order transition. Of coarse, the values of $\Delta\mu_{pw}(T)$ obtained in Figs. 1 and 2 coincide. Moreover, the points M_1 and M_2 merge into M_{cross}. The states along the C_1-M_{cross}-C_2 line are stable, while that lying in the sectors M_1-S_1 and S_2-M_2 are metastable. According to Hansen and McDonald, this kind of metastable states could be reached experimentally if sufficiently care is taken to prevent formation of the thermodynamically stable phase (see Chap. 5.6 in Ref. 29).

Figure 3(a) shows adsorption isotherms for Xe/Na evaluated at several temperatures above T_w. Horizontal lines indicate $\Delta\mu_{pw}(T)$ determined from Maxwell constructions described above. One may observe the evolution of the PW phenomenon characterized by the jump in coverage $\Delta\Gamma_\ell = \Gamma_{\ell,\,max} - \Gamma_{\ell,\,min}$ (or equivalently $\Delta n = n_{max} - n_{min}$) at $\Delta\mu_{pw}(T)$. The largest jump occurs close to T_w, it shrinks for increasing T and eventually disappears at T_{cpw} where the thin and thick films merge. The temperature dependence of $\Delta\mu_{pw}(T)$ is shown in Fig. 3(b). This kind of PW line corresponds to

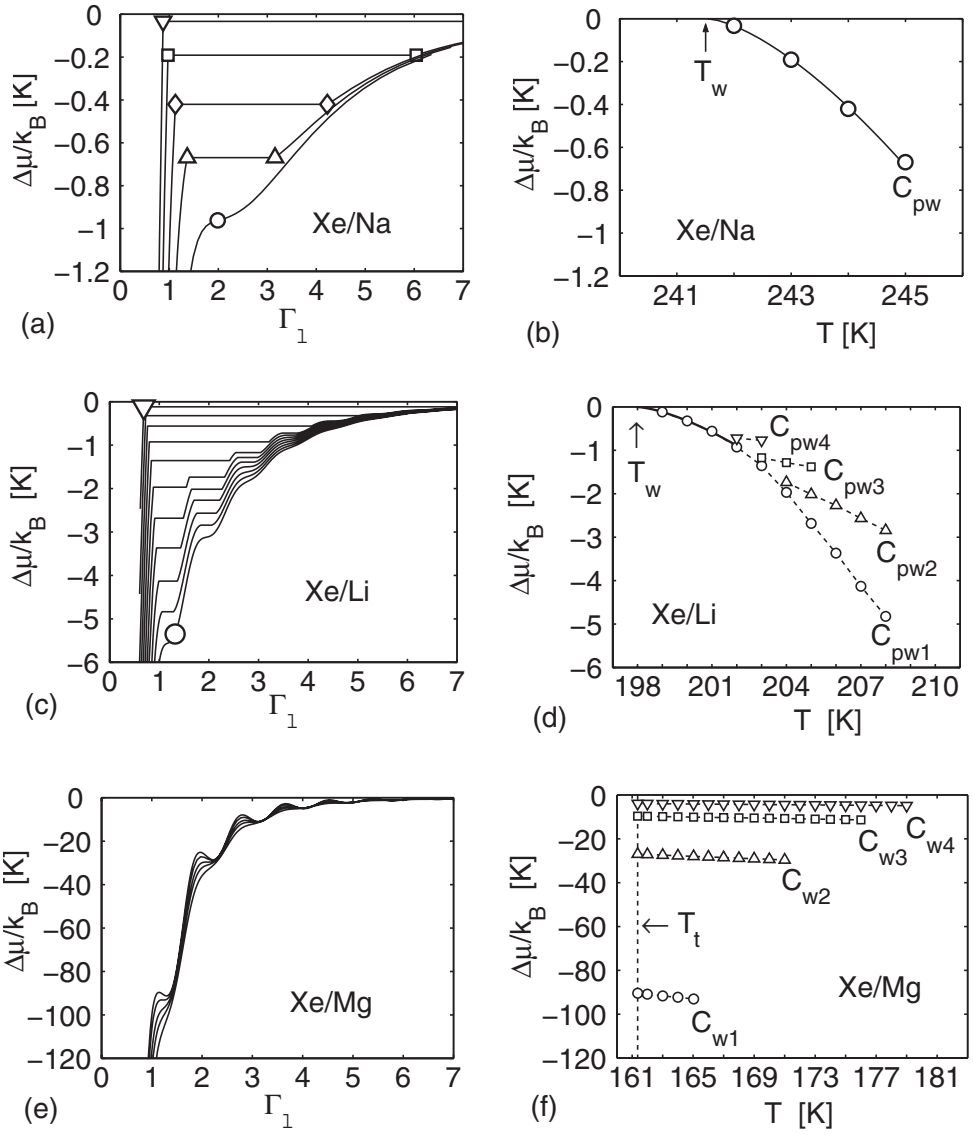

FIG. 3. (a) Adsorption isotherms for Xe adsorbed on a single wall of Na as a function of coverage Γ_ℓ at temperatures from 242 K (triangle-down) to 246 K (circle) in steps of 1 K. (b) PW line for the Xe/Na system. The solid curve is the tangential fit. (c) Same as (a) for Xe/Li at T from 199 K (triangle-down) to 209 K (circle). (d) Phase diagram for Xe/Li. (e) Same as (a) for Xe/Mg at several values of T from T_t to 184 K. (f) Phase diagram for Xe/Mg.

the cases depicted in panel (a) of Fig. 20 in Ref. 2 and in panel (b) of Fig. 1 in Ref. 3 and it has been measured in several systems.[1] This quantity approaches tangentially zero at T_w, thermodynamic arguments[3] leads to the form

$$\Delta\mu_{pw}(T) = \mu_{pw}(T) - \mu_0(T) = a_{pw}\,(T - T_w)^{3/2}\,, \tag{28}$$

with a_{pw} being a model parameter. In practice, this expression is used to fit data of $\Delta\mu_{pw}(T)$ for determining T_w. In the case of Xe/Na we obtained $T_w = 241.6$ K and $a_{pw}/k_B = -0.12$ K$^{-1/2}$. In addition, Fig. 3(a) fixes an upper limit for the CPW point at $T_{cpw} \lesssim 246$ K.

Adsorption isotherms for the Xe/Li system are displayed in Fig. 3(c). In this case the equal area Maxwell constructions yielded multiple jumps in coverage for a fixed T. In turn, this feature led to a series of merging PW lines. These lines are plotted in Fig. 3(d), the exhibited features are similar to that shown in panel (c) of Fig. 20 in Ref. 2 and in panel (d) of Fig. 1 in Ref. 3. One

may observe a series of surface triple points which determine a line of coalescence. The fit of this line to Eq. (28) yielded $T_w = 198.0$ K and $a_{pw}/k_B = -0.11$ K$^{-1/2}$. The present T_w is lower than the value $T_w = 225$ K quoted in Table I of Ref. 27 obtained from GCMC calculations. In this context, it becomes important to notice that our calculations[17] predict wetting of Rb by Ne in agreement with the experimental result of Hess, Sabatini, and Chan,[45] while the GCMC result reported in Table I of Ref. 27 suggests drying for Ne/Rb indicating that in such GCMC calculations the wetting properties are shifted toward higher T.

Adsorption isotherms calculated for Xe/Mg are displayed in Fig. 3(e). Since Maxwell constructions cannot be separated on the scale of the drawing they are not shown. These data don't exhibit a "standard" PW pattern because Mg is significantly more attractive than the alkali metals. A layer-by-layer film growth for $T \geq T_t$ may be observed. The corresponding phase diagram is plotted in Fig. 3(f) being similar to that depicted in Fig. 16(a) of Ref. 2 for strong substrates.

B. Filling a planar slit pore

In the slit geometry Xe atoms are confined by two identical solid walls separated by a distance L. Hence, the *s-f* interaction becomes $U_{sf}(z) = U_{\rm CCZ}(z) + U_{\rm CCZ}(L - z)$ and repulsion at the walls leads to $\rho(z = 0) = \rho(z = L) = 0$. The reported solutions of the E-L equations correspond to a slit with $L^* = 40$. This width is wider than $L^* = 29.1$ adopted for the pioneering molecular dynamics calculations[4] guaranteeing that the direct pair interaction between two atoms located close to opposite walls be negligible. First, we shall deal with closed systems and next to discuss the results for open slits.

1. Closed slits - Canonical ensemble

We shall now describe the filling of closed slits, i.e. systems at constant n, performed at fixed T and V. In this case, the equilibrium states were determined by adopting the CE statistics. Symmetric and asymmetric solutions were obtained along PW lines found in Sec. III A.

Let us first look at the results for a slit of Na at $T = 245$ K. The adsorption isotherm is displayed in Fig. 4. Symmetric solutions indicated by the curve running through the points $C_{S1}, S_{S1}, S_{S2}, C_{S2}$ exhibit the same pattern like that displayed in Fig. 1 for a single wall adsorption. Moreover, as expected the same values of the reduced chemical potential $\Delta\mu$ are obtained for abscissas $\Gamma_\ell(slit) = 2\,\Gamma_\ell(wall)$. In addition, there are asymmetric solutions along the curve determined by the points S_{S1}, S_{A1}, S_{A2}. The difference between the free energies per particle, $f_{\rm DF} = F_{\rm DF}/N$, of asymmetric and symmetric solutions obtained at $T = 245$ K is displayed as a function of Γ_ℓ in Fig. 5. The asymmetric solutions have lower free energies than the symmetric ones over the entire range S_{S1}-S_{A2}. This feature is obtained at all temperatures in the range $T_w < T < T_{sb}$. All internal states between the spinodal points S_{S1} and S_{S2} with minimum free energy could be stabilized in a closed slit pore.[43]

In order to facilitate comparisons between results for different absorbers, the main findings are depicted in a compact manner in Fig. 6. Panels (a)-(e) show that the asymmetric $\rho(z)$ appear after a thin dense layer was adsorbed on both walls, similarly to the profile plotted in Fig. 3 of Ref. 6.

Figure 6(a) shows the asymmetric filling of a slit of Na at $T = 245$ K, data for various Γ_ℓ are displayed. The asymmetry of the density profiles is measured by the quantity

$$\Delta_N(\%) = \frac{100}{n} \int_0^{L/2} dz\, [\rho(z) - \rho(L - z)]\ . \tag{29}$$

In fact, there are two energetically equivalent asymmetric solutions which satisfy $\rho_{asym2}(z) = \rho_{asym1}(L - z)$ yielding $\Delta_N[\rho_{asym2}] = -\Delta_N[\rho_{asym1}]$. The obtained values of Δ_N for $T \geq T_w$ are displayed in Fig. 6(f). A look at this drawing indicates that, at a fixed T, asymmetric $\rho(z)$ appear between a lower and an upper coverage limit and this jump diminishes with increasing temperatures. Furthermore, we can state that the SSB effect extends along the single PW line displayed in Fig. 3(b) terminating at a critical T_{sb}, which coincides with T_{cpw}.

In the case of Xe/Li we show results obtained at $T = 205$ K. This value of T was selected because it is the highest temperature exhibiting three first-order transition lines. Panels (b), (c), and (d) of Fig. 6 show the asymmetric formation of the second, third, and fourth layer. These structures

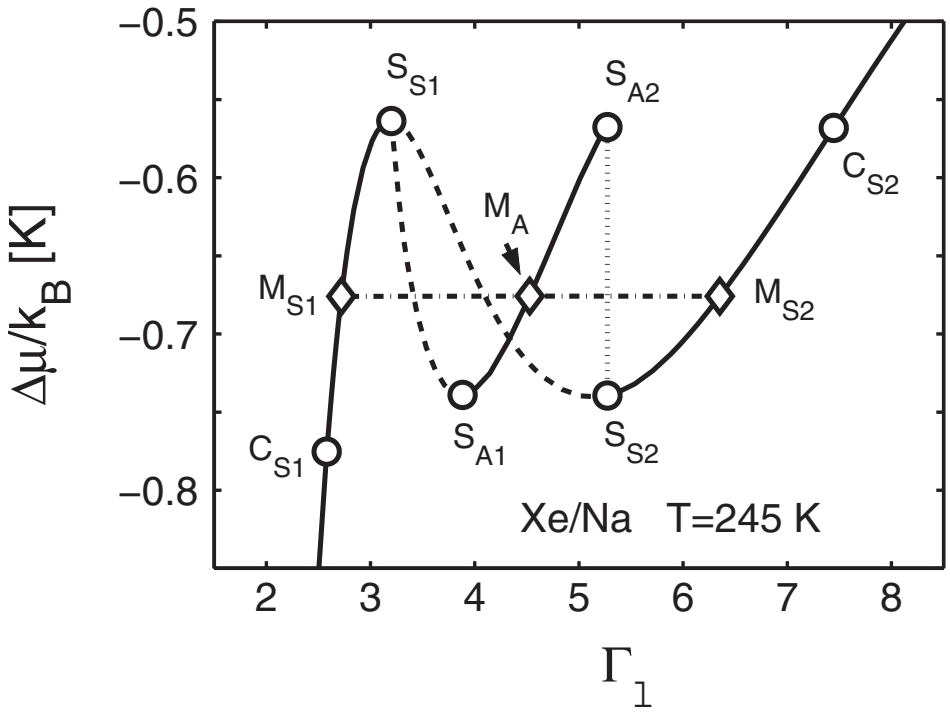

FIG. 4. Adsorption isotherm for symmetric and asymmetric solutions plotted as the reduced chemical potential versus coverage Γ_ℓ. The symmetric solutions go through the set of points $(C_{S1}, S_{S1}, S_{S2}, C_{S2})$, while the asymmetric ones join the points $(S_{S1}, S_{A1}, S_{A2}, S_{S2})$. The horizontal line is the Maxwell construction joining the symmetric stable coexistent states M_{S1} and M_{S2}, whilst M_A stands for the asymmetric stable coexistent state (see text).

can be related, respectively, to the PW lines denoted by C_{pw1}, C_{pw2}, and C_{pw3} in the $(T,\Delta\mu)$ plane depicted in Fig. 3(d). A comparison of the asymmetry coefficients displayed in Fig. 6(g) and the first-order transition lines plotted in Fig. 3(d) indicates that the corresponding values of T_{sb} and T_{cpw} coincide. The chemical potential for both kind of solutions is displayed in Fig. 6(h). These van der Waals loops indicate that asymmetric solutions begin at a relative maximum of μ_{sym} and finish at the next relative minimum. So, asymmetry appears just in the region where the slope of μ_{sym} is negative implying instability of the symmetric solutions, whilst the slope of μ_{asym} is positive over a large portion of that region satisfying the stability condition there. Figure 6(i) shows a comparison of $f_{\rm DF}$ of symmetric (circles) and asymmetric (triangles) states for $n = 0.165$ [corresponding to $\Gamma_\ell = 2.33$ where Δ_N reaches its maximum at $T = 208$ K, see Fig. 6(g)], the data correspond to temperatures $T = 205$, 206, 207, and 208 K. To get a comparison on the same scale the data were shifted by a constant $f_{\rm const}(T)$ at each temperature, hence, we plotted $\Delta f_{\rm DF} = f_{\rm DF} - f_{\rm const}(T)$. It is clear that the $\Delta f_{\rm DF}$ of the asymmetric solutions is lower than that of symmetric one. This behavior is extended to other values of Γ_ℓ. A crude estimation of an energy barrier between asymmetric to symmetric states was performed by assuming at fixed T and n the path $\rho(z) = (1-\alpha)\rho_{asym}(z) + \alpha\,\rho_{sym}(z)$ with α running from 0 to 1. Both the free energy, $\Delta f_{\rm DF}$, and the asymmetry coefficient, Δ_N, were evaluated as a function of α. These results are also displayed in Fig. 6(i). The barrier diminishes for increasing T and disappears at $T = 209$ K.

For Xe/Mg the asymmetric solutions also occur along the first-order transition lines displayed in Fig. 3(f). Figure 6(e) shows the asymmetric formation of the second layer in a slit of Mg at T_t. The asymmetry parameter for T_t, T_{nb}(normal boiling T)=165.03 K, 171 K, and 176 K is plotted in Fig. 6(j) as a function of coverage. This picture indicates that, as before, the values of T_{sb} coincide with the end temperatures of the corresponding C_{wi} lines.

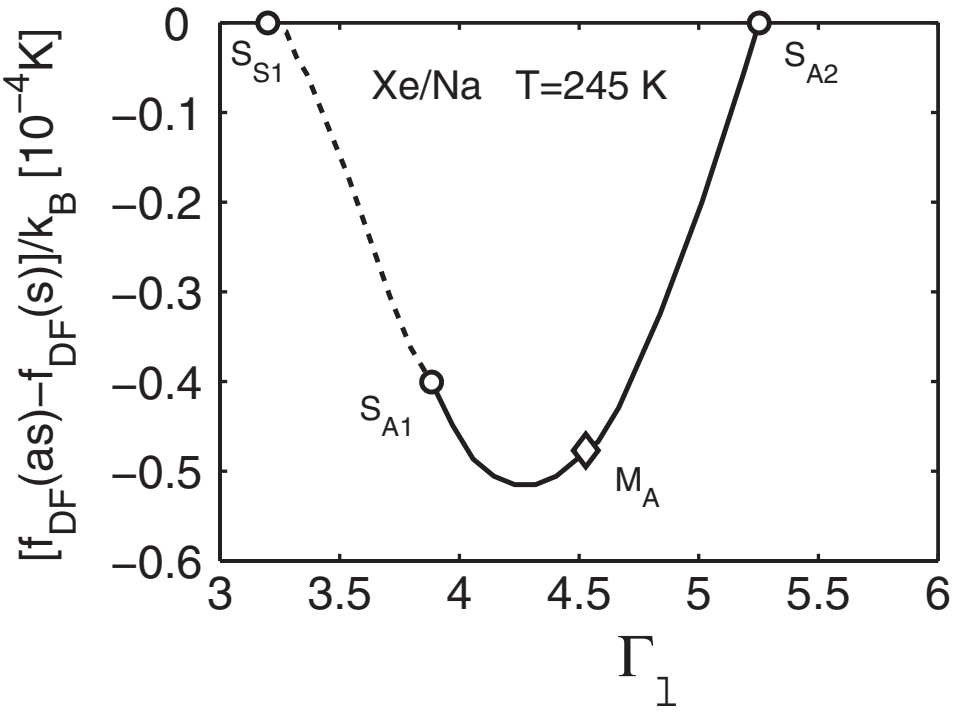

FIG. 5. Difference between free energies per particle of asymmetric and symmetric solutions obtained in the CE frame as a function of coverage Γ_ℓ. Labels S_{S1}, S_{A1}, S_{A2} and M_A have the same meaning as in Fig. 4. In the regime delimited by S_{A1} and S_{A2} the chemical potential of asymmetric solutions exhibits a positive slope and these results are also obtained in the GCE scheme.

2. Grand canonical ensemble

Open slits are also in thermodynamic equilibrium with an environment at fixed T, but in this case the confined system is exposed to an unrestricted fluid exchange with the reservoir at fixed μ. Under such circumstances, the adsorption occurs at constant V, T, and μ. Therefore, as mentioned before the adequate procedure for studying this phenomenon is to use GCE.

Let us now comment the results for the same system analyzed in detail in the previous section, i.e. Xe/Na at $T = 245$ K. All the states marked with solid lines in Fig. 4 were also obtained from GCE calculations. Hence, GCE **does** provide both symmetric as well as asymmetric solutions in the regimes where the corresponding Helmholtz free energy, $F_{\rm DF}$, is convex yielding positive $d\mu/dn$. The lack of data in the non convex region makes it necessary to apply the crossing method for searching the coexistent states. Figure 7 shows μ as a function of ω for both symmetric and asymmetric solutions corresponding to data displayed in Fig. 4. The crossing of the lines labeled by C_{S1}-S_{S1} and S_{S2}-C_{S2} at M_{cross} in Fig. 7 determines the coexistent symmetric solutions M_{S1} and M_{S2} already quoted in Fig. 4. Furthermore, the line S_{A1}-S_{A2} corresponding to asymmetric solutions crosses the symmetric ones also just at M_{cross}. So, the state M_A included in Fig. 4 has the same ω_e like the coexistent symmetric states M_{S1} and M_{S2}. This means that M_{cross} is a triple point determined by the intersection of three lines, where the three phases in equilibrium satisfy

$$\mu_{S1}(T, \omega_e) = \mu_{S2}(T, \omega_e) = \mu_A(T, \omega_e) = \mu_e(T, \omega_e) \ . \tag{30}$$

The density profile of the state M_A is marked with a fat line in Fig. 6(a). In passing, let us mention that for completeness this state was also included in Fig. 5. The density profiles of the states M_{S1}, M_A, and M_{S2} are compared in Fig. 8. In the symmetric cases M_{S1} and M_{S2} the film formed at each wall coincides, respectively, with the thin and thick structures got at coexistence for adsorption on a single wall. On the other hand, for M_A one may observe at the right wall the coexistent thick film

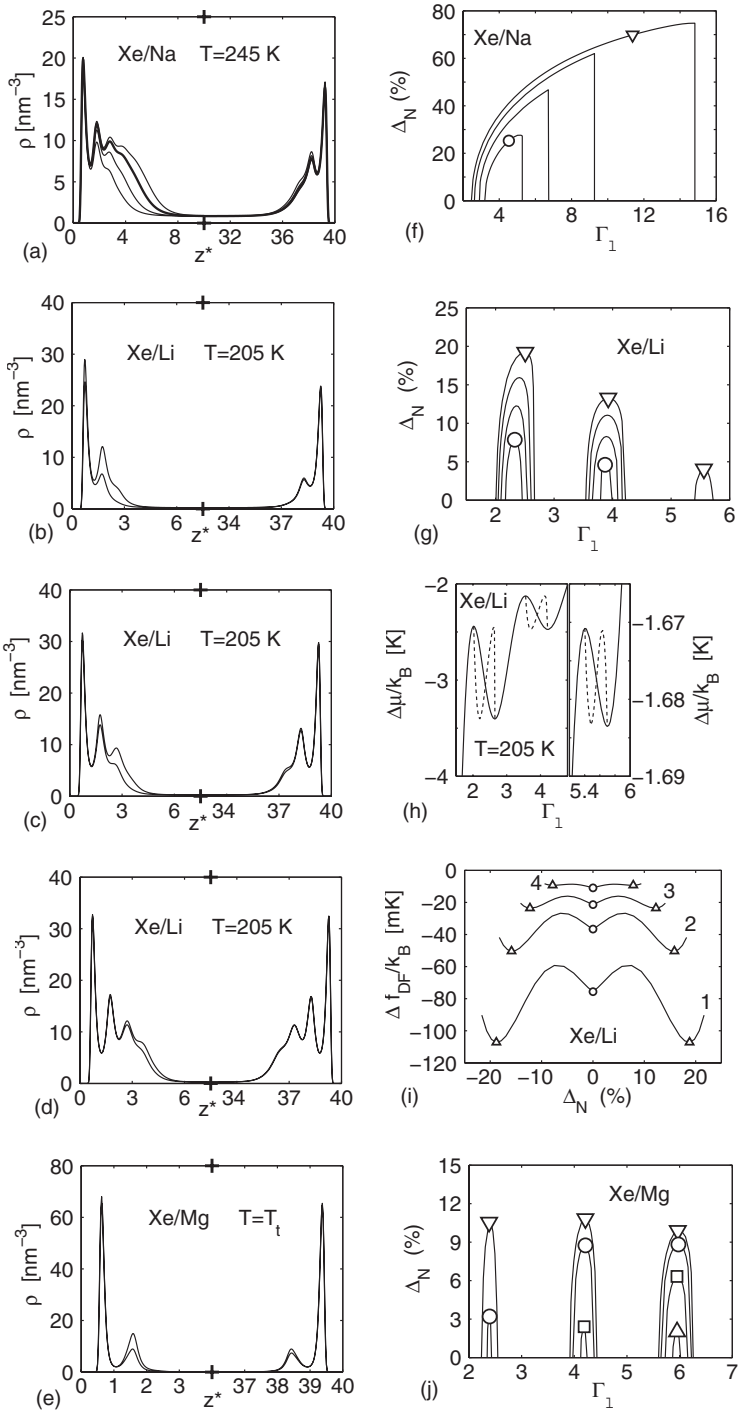

FIG. 6. (a) Asymmetric density profiles of Xe near to walls of a closed slit of Na at $T = 245$ K for coverages $\Gamma_\ell = 3.23$, 3.79, 4.53 and 5.19. (b) Same as (a) for Xe/Li at $T = 205$ K for $\Gamma_\ell = 2.04$ and 2.43. (c) Same as (b) for $\Gamma_\ell = 3.55$ and 3.85. (d) Same as (b) for $\Gamma_\ell = 5.44$ and 5.58. (e) Same as (a) for Xe/Mg at $T = T_t$ for $\Gamma_\ell = 2.24$ and 2.42. (f) Asymmetry parameter for Xe/Na as a function of coverage at temperatures from 242 K (triangle-down) to 245 K (circle) in steps of 1 K. (g) Same as (f) for Xe/Li at T from 205 K (triangle-down) to 208 K (circle). Data correspond to the asymmetric filling of the first four layers. (h) Chemical potential for Xe/Li at $T = 205$ K as a function of coverage. Solid and dashed curves correspond to symmetric and asymmetric solutions, respectively. (i) Relative free-energy per particle for Xe/Li showing energy barriers between symmetric (circles) and asymmetric (triangles) states at $T = 205$, 206, 207, and 208 K labeled by 1, 2, 3, and 4, respectively. (j) Same as (f) for Xe/Mg at $T = T_t$ (triangle-down), T_{nb} (circle), 171 K (triangle-up), and 176 K (square).

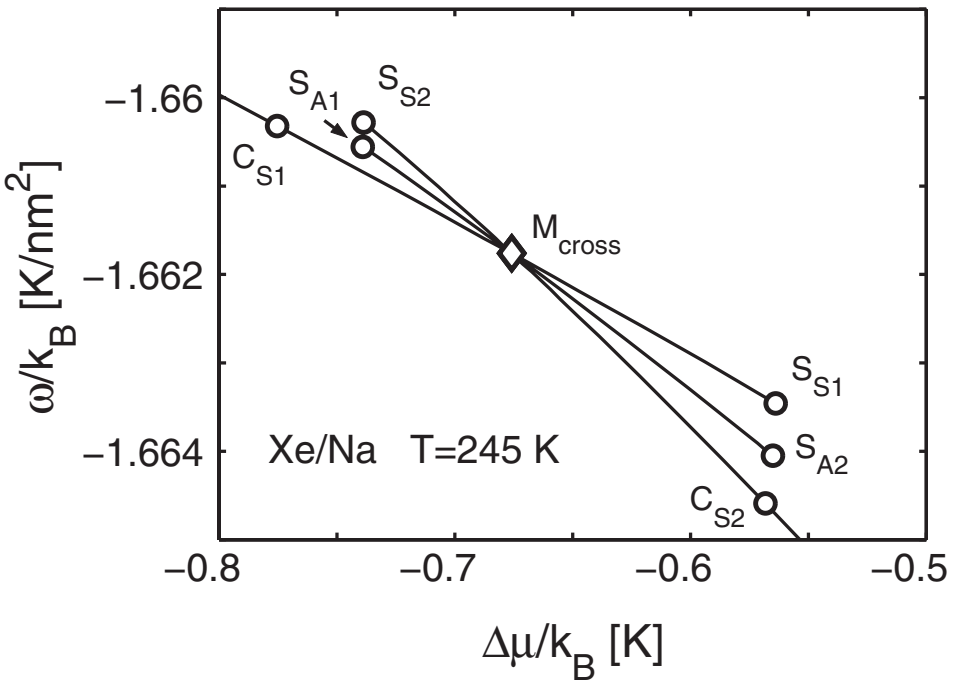

FIG. 7. Grand free energy per unit one wall area as a function of the reduced chemical potential for symmetric and asymmetric solutions. The meaning of points ($C_{S1}, S_{S1}, S_{A1}, S_{A2}, S_{S2}, C_{S2}$) is the same as in Fig. 4. The symmetric solutions lay on the curves C_{S1}-S_{S1} and S_{S2}-C_{S2}, while the asymmetric determine the line S_{A1}- S_{A2} The point M_{cross} indicates the location of the crossing the three lines determining the coexistence of symmetric and asymmetric solutions labeled, respectively, by M_{S1}, M_{S2}, and M_A in Fig. 4.

and at the other wall the coexistent thin film. Notice that the asymmetric solution is twofold, it can also present a thin film at the right wall and a thick film at the left one.

It is important to notice that data plotted in Fig. 7 indicate that, away from M_{cross} for each value of $\Delta\mu$ the asymmetric metastable states have always lower grand potential energy, ω, than the symmetric metastable ones. On the other hand, above T_w for a given μ the states with lowest grand potential lay on the curves denoted by C_{S1}-M_{cross}-C_{S2} and their structures are uniform films along the (x,y) plane. Therefore, no structure breaking symmetry on the (x,y) plane would have lower ω at μ_e than the coexistent symmetric and asymmetric states obtained at M_{cross}.

At lower values of T the system Xe/Na exhibits similar features to that found at $T = 245$ K. One also gets triple points where symmetric and asymmetric states coexist. Figure 9 shows the envelope of coexistence for temperatures $T > T_w$. These data were obtained in both the CE and GCE frames. One may realize that the coverage Γ_ℓ corresponding to the symmetric thick films as well as to the asymmetric ones goes to infinity when the temperature approaches T_w. On the other hand, both symmetric and the asymmetric one merge at T_{cpw} located slightly below $T = 246$ K. Above this temperature only one sort of symmetric states are obtained.

The results obtained for the isotherms for Xe/Na analyzed above can be extended to any other series van der Waals loops found for systems Xe/Li and Xe/Mg examined in Sec. III B 1. Moreover, all the features remain unchanged when the width of the slit is enlarged. The results for the system Ar/Li reported in Ref. 12 give support to the latter statement.

IV. SUMMARY

Adsorption of Xe on alkaline planar surfaces was investigated within the frame of a DF theory. Namely, physisorption on single walls and filling of symmetric slit pores were analyzed. Both the CE and GCE statistics were applied.

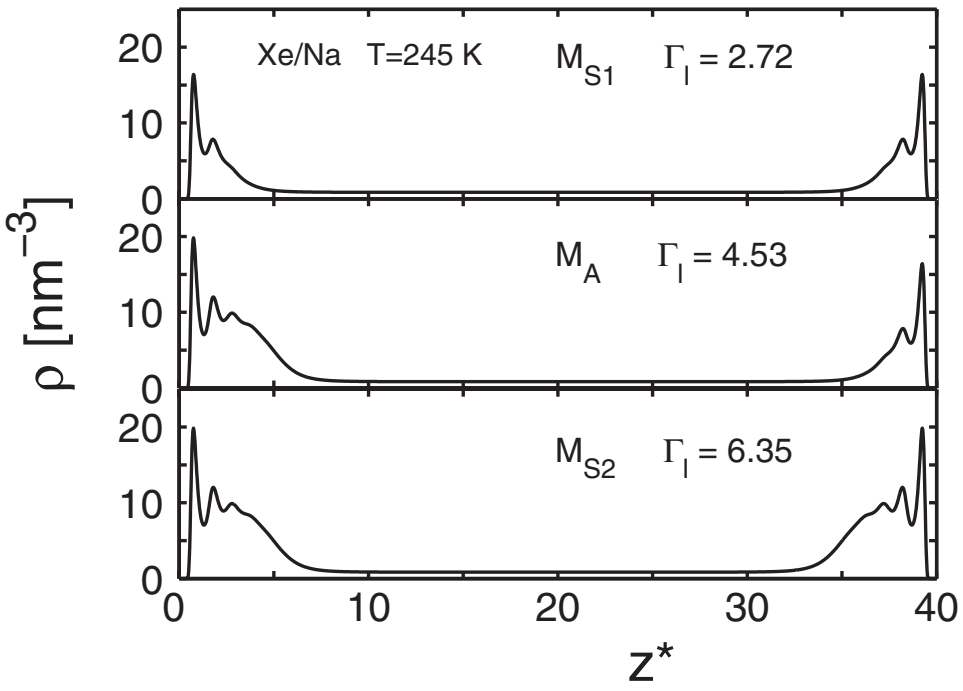

FIG. 8. Density profiles of Xe confined in a slit of Na as a function of z. These data correspond to coexistent systems in the GCE statistics at $T = 245$ K. The labels M_{S1} and M_{S2} indicate symmetric solutions, while M_A indicates the asymmetric one.

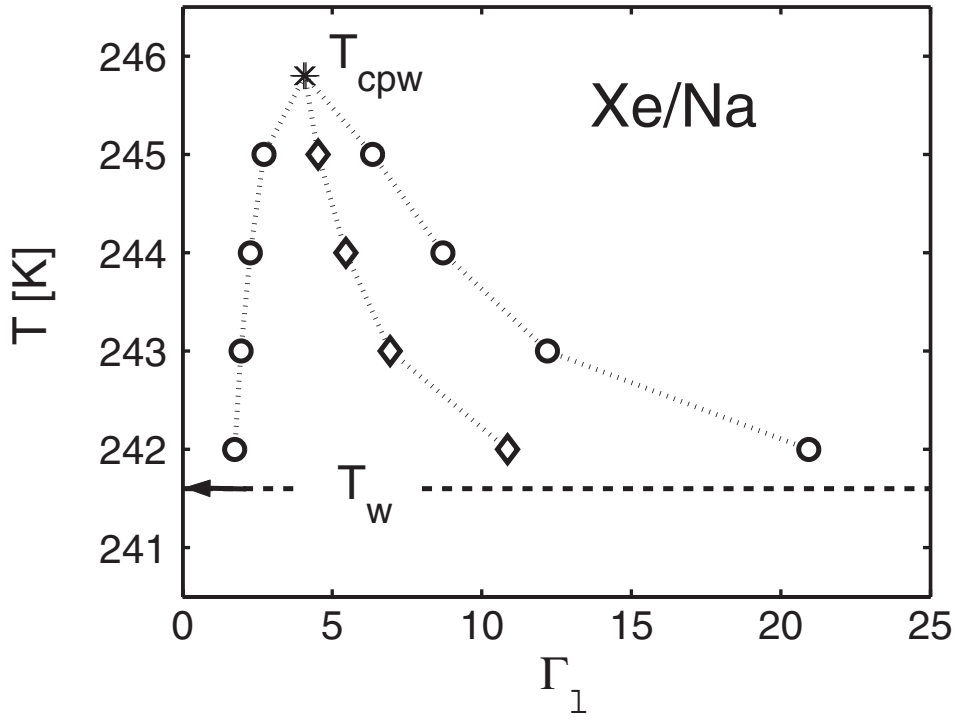

FIG. 9. Coexistent states of Xe confined in a slit of Na at temperatures between T_w and T_{cpw}. These data were obtained with both the CE and GCE statistics. Circles are symmetric states, while diamonds are asymmetric ones. The dotted lines are plotted to guide the eye, all these there lines merge at T_{cpw} indicated by the asterisk.

Calculations for adsorption on a single wall were performed in order to identify first-order phase transitions and determining PW lines. Equilibrium chemical potential μ_e at which stable thin and thick films coexist were evaluated by applying Maxwell constructions (equal area procedure for CE and crossing technique for GCE). The obtained results at coexistence with CE and GCE are equal. PW lines were used to determine wetting temperatures T_w.

The filling of closed slits of identical walls was studied at temperatures higher than T_w by applying the CE scheme. Solutions breaking the left-right symmetry of the adsorption potential exerted by the slit appear in the range of Γ_ℓ corresponding to $\Delta\mu$ of PW lines appear. Between spinodal points of the symmetric solutions the asymmetric profiles exhibit a lower Helmholtz free energy than the symmetric ones for the same number of particles. Therefore, these SSB species could be stabilized in a closed system.

Open slits were studied within the GCE frame. All the symmetric and asymmetric states with positive $d\mu/dn$ provided by the CE scheme were also obtained when applying GCE. The crossing Maxwell construction yielded three coexistent states with the same ω and μ, i.e, two symmetric and one asymmetric twofold degenerate. The symmetric solutions exhibit at both walls either the thin or the thick film obtained at coexistence in the adsorption on a single wall. While the asymmetric state shows at the left wall the coexistent thick film and at the right wall the corresponding thin one, or vice versa. These results indicate that given a sort "coexistent film" at one wall it is no matter whether at the other wall one has the "thin" or the "thick coexistent film". This finding is a realization in a realistic system of a behavior qualified as conceivable by Merkel and Löwen in the introduction of Ref. 14.

On the basis of the present DF calculations we conjecture that for $T \geq T_w$ there is a one-to-one correspondence between any first-order phase transition line and the occurrence of asymmetric filling. In the case of complex phase diagrams like those of Fig. 3(d) and 3(f) corresponding to layering transitions, a multiple entrance of SSB at a fixed T was found. Moreover, the coincidence of the CPW points where the PW lines terminate and the critical temperatures T_{sb} at which asymmetric solutions disappear is clearly established.

Below T_w one expects that asymmetric profiles with lowest free energy shall also break the symmetry in the (x,y) plane exhibiting structures like those obtained in Refs. 9 and 16.

To the best of our knowledge these findings supporting a very close relation between wetting and filling have not been reported before. Moreover, this kind of SSB might appear in other theoretical frames which look symmetrical. Since the present work deals with realistic systems, the properties described above are sufficiently relevant to encourage experimental verification. Perhaps, such SSB profiles could be observable in confined colloidal suspensions.

ACKNOWLEDGMENTS

This work was supported in part by grants PICT 31980/05 from ANPCyT, PIP 0546/09 from CONICET, and X099 from Universidad de Buenos Aires, Argentina.

[1] *Special Issue: Wetting, Spreading and Filling*, Guest Eds. M. S. Petersen and M. W. Cole, J. Low Temp. Phys. **157**, 75 (2009).
[2] R. Pandit, M. Schick, and M. Wortis, "Systematics of multilayer adsorption phenomena on atttractive substrates," Phys. Rev. B **26**, 5112-5140 (1982); and citations therein.
[3] R. Pandit and M. E. Fisher, "Wetting transitions near bulk triple points," Phys. Rev. Lett. **51**, 1772-1775 (1983).
[4] J. H. Sikkenk, J. O. Indekeu, J. M. J. van Leeuwen, and E. O. Vossnack, "Molecular-dynamics simulation of wetting and drying at solid-fluid interfaces," Phys. Rev. Lett. **59**, 98-101 (1987).
[5] J. H. Sikkenk, J. O. Indekeu, J. M. J. van Leeuwen, E. O. Vossnack, and A. F. Bakker, "Simulation of wetting and drying at solid-fluid interfaces on the Delft molecular dynamics processor," J. Stat. Phys. **52**, 23-44 (1988).
[6] J. Z. Tang and J. G. Harris, "Fluid wetting on molecularly rough surfaces," J. Chem. Phys. **103**, 8201-8208 (1995).
[7] G. O. Berim and E. Ruckenstein, "Symmetry breaking of the fluid density profiles in closed nanoslits," J. Chem. Phys. **126**, 124503 (2007).
[8] L. Szybisz, and S. A. Sartarelli, "Density profiles of Ar adsorbed in slits of CO_2: Spontaneous symmetry breaking revisited," J. Chem. Phys. **128**, 124702 (2008).
[9] G. O. Berim, and E. Ruckenstein, "Two-dimensional symmetry breaking of fluid density distribution in closed nanoslits," J. Chem. Phys. **128**, 024704 (2008).

[10] S. A. Sartarelli and L. Szybisz, "Correlation between asymmetric profiles in slits and standard prewetting lines," Papers in Physics **1**, 010001 (2009) [also at http://arxiv.org/abs/0909.2244].
[11] S. A. Sartarelli, L. Szybisz, and I. Urrutia, "Spontaneous symmetry breaking and first-order phase transitions of adsorbed fluids," Int. J. Bifurcation Chaos **20**, 287-294 (2010).
[12] S. A. Sartarelli and L. Szybisz, "Confinement of Ar between two identical parallel semi-infinite walls," J. Chem. Phys. **132**, 064701 (2010).
[13] G. O. Berim, and E. Ruckenstein, "Symmetry breaking of the density distribution of a quantum fluid in a nanoslit," J. Chem. Phys. **131**, 184707 (2009).
[14] M. Merkel and H. Löwen, "Symmetry-breaking density profiles in confined liquids," Phys. Rev. E **54**, 6623-6632 (1996).
[15] W. Rzysko, A. Patrykiejew, and S. Sokołowski, "Nucleation of fluids confined between parallel walls: A lattice Monte Carlo study," Phys. Rev. E **77**, 061602 (2008).
[16] J. R. Edison and P. A. Monson, "Modeling relaxation processes for fluids in porous materials using dynamic mean field theory: An Application to partial wetting," J. Low Temp. Phys. **157**, 395-409 (2009).
[17] S. A. Sartarelli, L. Szybisz, and I. Urrutia, "Adsorption of Ne on alkali surfaces studied with a density functional theory," Phys. Rev. E **79**, 011603 (2009).
[18] S. A. Sartarelli and L. Szybisz, "Adsorption of Ar on planar surfaces studied with a density functional theory," Phys. Rev. E **80**, 052602 (2009).
[19] R. Evans, in *Fundamentals of Inhomogeneous Fluids*, ed. D. Henderson (Decker, New York, 1992).
[20] P. Hohenberg and W. Kohn, "Inhomogeneous electron gas," Phys. Rev. **136**, B864-B871 (1964).
[21] F. Ancilotto, S. Curtarolo, F. Toigo, and M. W. Cole, "Evidence concerning drying behavior of Ne near a Cs surface," Phys. Rev. Lett. **87**, 206103 (2001).
[22] E. Kierlik and M. L. Rosinberg, "Free-energy density functional for inhomogeneous hard-sphere fluid: Application to interfacial adsorption," Phys. Rev. A **42**, 3382-3387 (1990).
[23] Y. Rosenfeld, "Free-energy model for the inhomogeneous hard-sphere fluid mixture and density-functional theory of freezing," Phys. Rev. Lett. **63**, 980-983 (1989).
[24] R. Roth, R. Evans, A. Lang, and G. Kahl, "Fundamental measure theory for hard-sphere mixture revisited: the White Bear version," J. Phys.: Condens. Matter **14**, 12063-12078 (2002).
[25] G. A. Mansoori, N. F. Carnahan, K. E. Starling, and T. W. Leland Jr, "Equilibrium thermodynamic properties of the mixture of hard spheres," J. Chem. Phys. **54**, 1523-1525 (1971).
[26] J. D. Weeks, D. Chandler, and H. C. Andersen, "Role of repulsive forces in determining the equilibrium structure of simple liquids," J. Chem. Phys. **54**, 5237-5247 (1971).
[27] S. Curtarolo, G. Stan, M. J. Bojan, M. W. Cole, and W. A. Steele, "Threshold criterion for wetting at the triple point," Phys. Rev. E **61**, 1670-1675 (2000).
[28] V. A. Rabinovich, A. A. Vasserman, V. I. Nedostup, and L. S. Veksler, *Thermophysical properties of neon, argon, krypton, and xenon* (Hemisphere, Washington, DC, 1988).
[29] J.-P. Hansen and I. R. McDonald, *Theory of simple fluids* (Elsevier, Amsterdam, 2006).
[30] S. Sokołowski and J. Stecki, "Second surface virial coefficient for argon adsorbed on graphite," J. Phys. Chem. **85**, 1741-1746 (1981).
[31] B. L. Smith, P. R. Gardner, and E. H. C. Parker, "Surface tension and energy of liquid xenon," J. Chem. Phys. **47**, 1148-1152 (1967); J. Zollweg, G. Hawkins, and G. B. Benedek, "Surface tension and viscosity of xenon near its critical point," Phys. Rev. Lett. **27**, 1182-1185 (1971).
[32] A. Chizmeshya, M. W. Cole, and E. Zaremba, "Weak biding potentials and wetting transitions," J. Low Temp. Phys. **110**, 677-682 (1998).
[33] O. Sinanoğlu and K. S. Pitzer, "Interactions between molecules adsorbed on a surface," J. Chem. Phys. **32**, 1279-1288 (1960).
[34] L. W. Bruch, M. W. Cole, and E. Zaremba, *Physical Adsorption: Forces and Phenomena* (Clarendon press, Oxford, 1997) [Chap. 2.3.2.2].
[35] F. Ancilotto and F. Toigo, "Prewetting transitions of Ar and Ne on alkali-metal surfaces," Phys. Rev. B **60**, 9019-9025 (1999).
[36] P. I. Ravikovitch, A. Vishnyakov, and A. V. Neimark, "Density functional theories and molecular simulations of adsorption and phase transitions in nanopores," Phys. Rev. E **64**, 011602 (2001).
[37] M. Zeng, Y. Tang, J. Mi, and C. Zhong, "Improved direct correlation function for density functional theory analysis of pore size distributions," J. Phys. Chem. C **113**, 17428-17436 (2009).
[38] L. Szybisz and M. L. Ristig, "New method of solving the optimized paired-phonon analysis equations and stability of thin films of liquid ^{4}He at $T = 0$ K," Phys. Rev. B **40**, 4391-4404 (1989).
[39] B. E. Clements, E. Krotscheck, and H. J. Lauter, "Growth instability in helium films," Phys. Rev. Lett. **70**, 1287-1290 (1993).
[40] W. M. Saslow, G. Agnolet, C. E. Campbell, B. E. Clements, and E. Krotscheck, "Theory of first-order layering transitions in thin helium films," Phys. Rev. B **54**, 6532-6538 (1996).
[41] L. Szybisz,, "Confirmation using Monte Carlo ground-state energies of the instability of free planar films of liquid ^{4}He at $T = 0$ K," Phys. Rev. B **58**, 109-112 (1998).
[42] J. A. White, A. González, F. L. Román, and S. Velasco, "Density-functional theory of inhomogeneous fluids in the canonical ensemble," Phys. Rev. Lett. **84**, 1220-1223 (2000).
[43] A. V. Neimark, P. I. Ravikovitch, and A. Vishnyakov, "Inside the hysteresis loop: Multiplicity of internal states in confined fluids," Phys. Rev. E **65**, 031505 (2002).
[44] K. Huang, *Statistical mechanics* (Wiley, New York, 1963).
[45] G. B. Hess, M. J. Sabatini, and M. H. W. Chan, "Nonwetting of cesium by neon near its critical point," Phys. Rev. Lett. **78**, 1739-1742 (1997).